Available online at www.sciencedirect.com
SCIENCE DIRECT®
Pattern Recognition Letters 26 (2005) 27–41
Pattern Recognition Letters
www.elsevier.com/locate/patrec

A new accurate and flexible model based multi-corner detector for measurement and recognition

Gustavo Olague [a,*], Benjamín Hernández [b]

[a] *Proyecto EvoVisión, Departamento de Ciencias de la Computación, División de Física Aplicada, Centro de Investigación Científica y de Educación Superior de Ensenada, Km. 107 Carretera Tijuana-Ensenada, 22860, Ensenada, BC, Mexico*
[b] *Instituto de Astronomía, Universidad Nacional Autónoma de México Km. 103 Carretera Tijuana-Ensenada, 22830, Ensenada, BC, Mexico*

Received 26 August 2003; received in revised form 13 May 2004
Available online 28 October 2004

Abstract

This paper introduces a new parametric model capable of the modeling and identification of a certain class of characteristic intensity variations described by polygonal structures of a depicted 3D scene. We propose a new parametric corner modeling based on a Unit Step Edge Function (USEF) that defines a straight line edge. The USEF function is a distribution function, which models the optical and physical characteristics found in digital imaging systems. The simplicity of the model definition provides the flexibility and generality useful in modeling complex corners. Based on our model, we have been able to create a multi-corner detector using simple operations as addition and multiplication. Once we have built a detector, it is possible to retrieve the information useful in other machine vision tasks. An example of retrieving the position of a projected L-corner is developed. A new criterion for high-accurate L-corner localization is introduced, and a comparison with five previous corner criteria is made.

Keywords: Multi-corner modeling; Feature extraction; Corner detection; Nonlinear estimation theory; Analytical models

1. Introduction

Computer vision as well as close-range photogrammetry relies on image processing techniques in order to obtain the information required for tasks devoted to perceiving, sensing and measuring the world around a machine vision system.

* Corresponding author. Tel.: +52 646 1750500x25402; fax: +52 646 1750593.
E-mail addresses: olague@cicese.mx (G. Olague), benja@astrosen.unam.mx (B. Hernández).

0167-8655/$ - see front matter © 2004 Elsevier B.V. All rights reserved.
doi:10.1016/j.patrec.2004.08.026

A common paradigm to computer vision is the extraction of features described by specialized criteria depending on the task at hand. Feature extraction is one of the most important areas in computer vision. A great deal of effort has been spent by the computer vision and photogrammetric communities on this problem, see (Ackermann, 1984; Gruen, 1985; Foerstner, 1986; Medioni and Yasumoto, 1987; Gruen and Baltsavias, 1988; Mehrotra and Nichani, 1990; Rohr, 1992; Deriche and Giraudon, 1993; Rosin, 1996; Baker et al., 1998; Lindeberg, 1998; Tsai et al., 1999; Zheng et al., 1999), and in particular on the problem of edge detection, see (Moravec, 1977; Marr and Hildreth, 1980; Canny, 1986; Deriche, 1987). Corners are special features in images and are of great use in computing camera calibration, tracking, reconstruction and recognition, to mention but a few. Most gray scale corner detectors assume an idealized corner that is sharply pointed and has straight, steep edges and return just a single value measuring the "cornerity" or "strength" of the corner (e.g. Deriche, 1987; Harris and Stephens, 1988; Deriche and Giraudon, 1993; Mehrotra and Nichani, 1990; Zheng et al., 1999). However, corners rarely appears like this in the real world. Due to manufacturing limitations, wear and tear, streamlining, aesthetics, and so forth, corners are more typically rounded, blunted, blurred, ragged, textured, etc. Rosin has listed these attributes in more detail (Rosin, 1996). In particular, cornerity presents the following properties: Position or location, angle of aperture, orientation, edge shape, edge texture, contrast, edge profile, sharpness, color, junction type, and size. This paper introduces a new multi-corner image model based on straight lines that are merged using simple operators like addition and multiplication, see Olague and Hernández (2002). Our corner detector is a parametric based model detector, which provides with most of the above properties. A number of approaches have been proposed in the literature to solve the problem of corner extraction. In general, the approaches could be classified with respect to the level of accuracy of the detector, which could be obtained up to pixel or subpixel resolution. Examples of corner detectors designed for pixel resolution are: (1) Beaudet (1978) rotationally image operator, (2) Dreschler and Nagel (1982) based on local curvature extrema of region boundaries and (3) Kitchen and Rosenfeld (1982) based on the concept of Gaussian curvature. A drawback of these approaches is that they need a threshold. An approach for detecting edges is the use of the Laplacian-of-Gaussian (LoG), see (Marr and Hildreth, 1980). Deriche and Giraudon (1993) have introduced an approach combining the pro-perties of direct corner detectors and the localization behavior of the LoG for L-junctions. It is widely accepted that the position of the L-corner is extracted exactly and independently of the amount of blur. Indeed, Deriche and Giraudon approach is invariant to the blur factor. However, Deriche and Giraudon approach is not invariant with respect to the aperture angle, as we will show in this paper. Parametric based approaches (e.g. Baker and Nayar, 1998) are considered as gray level approaches as long as they work directly with the gray level image. Most of them aimed at detecting the corners within subpixel resolution. The appearance of such a feature in an image may well depend upon a number of parameters such as orientation, localization, scale, and level of blurring. The basic idea is to propose a parametric model and then fit the model directly to image intensities (Gruen, 1985). Rohr (1992) proposes a basic step function which is convolved with a Gaussian in order to model the blur. Deriche and Giraudon (1993) propose a corner detector similar to that of Rohr. A drawback of parametric based models to really be a paradigm that automatically constructs a detector is the lack of a suitable basic model. The basic model should provide the simpleness to build general complex models. The main contribution of this work is to present a new parametric model that due to its simplicity is able to provide the flexibility and generality for building any kind of complex corners. As a consequence of the new modeling, our model considers the blurring aspects within the basic model; therefore, it is not necessary to convolve the model with a Gaussian function. Rohr (1992) studied the displacement of the location using an analytical model of the corners, which introduces a smoothing procedure given by a Gaussian function that convolves with the corner model. The

objective of this work is to develop an algorithm that automatically constructs a feature detector for an arbitrary parametric feature. We concentrate our study here on L-corners and how the corner position is displaced for purpose of photogrammetric measurement. The approach can easily be extended to complex features for purpose of object recognition. Nevertheless, the displacement of complex features are more difficult to obtain due to the geometric reasoning used. The problem of L-corner detection is explained extensively in this paper. The displacement of the L-corner must be approached carefully in the case of a bandlimited system. This problem is of main concern for high accurate reconstruction. High-accurate corner extraction is a complex process due to the following factors: (1) the attitude, position and orientation, of the camera with respect to the object, (2) the interior orientation of the camera, (3) the fluctuations on illumination and (4) the camera optics, see (Olague, 2002). In this contribution we will use the concept that corners are always a subset of edges instead of adjacent surfaces. Surely, if three or more surfaces meet then there always be a corner. However, when two surfaces meet it is not clear whether is just a normal edge or an L-corner.

The paper is organized as follows: Section 2 introduces the new parametric based model, after which, we show how to build complex corners based on the basic model, including the L-corner and Vertex models. Section 5 introduces our criterion for precise corner location, which is based on purely geometric reasoning. Then, we compare analytically the L-corner localization problem with five previous corner detectors using our model. Finally, we calibrate our digital camera in order to show the benefits of using our high-accurate subpixel detector. We conclude the paper by summarizing the main contributions and mentioning how the new model could be used in future research.

2. Unit step edge function

Considering an image coordinate system $I(x,y)$ and an unknown set of parameters $P = (p_1,\ldots,p_n)$, the Unit Step Edge Function is constructed based on the error function definition.

Definition 1 (*Error function*). The error function, also called Gaussian probability integral, is a special case of the incomplete gamma function, and is commonly defined in C libraries. Its definition is:

$$\operatorname{erf}(x) = \frac{2}{\sqrt{\pi}} \int_0^x \mathrm{e}^{-t^2}\,\mathrm{d}t. \tag{1}$$

The function has the following limiting values and symmetries:

$$\operatorname{erf}(0) = 0, \quad \operatorname{erf}(\infty) = 1, \quad \operatorname{erf}(-x) = -\operatorname{erf}(x).$$

According to the above definition, we can derive a new function dividing the error function by 2 and adding half of a normal distribution in order to obtain a distribution function as follows:

$$\begin{aligned} F(x) &= \frac{1}{\sqrt{\pi}} \int_0^x \mathrm{e}^{-t^2}\,\mathrm{d}t + \frac{1}{\sqrt{2\pi}} \int_{-\infty}^0 \mathrm{e}^{\frac{-1}{2}t^2}\,\mathrm{d}t \\ &= \frac{\operatorname{erf}(x)}{2} + \frac{1}{2}. \end{aligned}$$

By replacing x appropriately we can derive the USEF definition along the x-axis.

Definition 2 (*Unit step edge function*). Let the image coordinates and the set of unknown model parameters be denoted by $I = (x,y)$ and $P_x = (p_{x1},\ldots,p_{xn})$, respectively. The unit step edge function is represented as follows:

$$U_x(I,P_x) = \pm \frac{1}{\sigma_1\sqrt{2\pi}} \int_0^x \mathrm{e}^{\frac{-(t-y\cdot\tan(\theta_1)-\mu_1)^2}{2\sigma_1^2}}\,\mathrm{d}t + \frac{1}{2}, \tag{2}$$

where the image coordinates are in the interval $[-m,m]$; the central point μ_1 designates the position x of the line that crosses along the y-axis; μ_1 lies in the interval $[-m,m]$; the rotation θ_1 is made clockwise about the (positive) y-axis; θ_1 designates the orientation of the edge model to be fitted to the image within the interval $-\frac{\pi}{2} < \theta_1 < \frac{\pi}{2}$; finally, a scaling factor σ_1 that characterizes the amount of blur introduced by the discretization process is included. σ_1 lies in the interval $[0,m]$. The unit edge function describes a distribution function that increases steadily from 0 to 1 with respect to the x-axis.

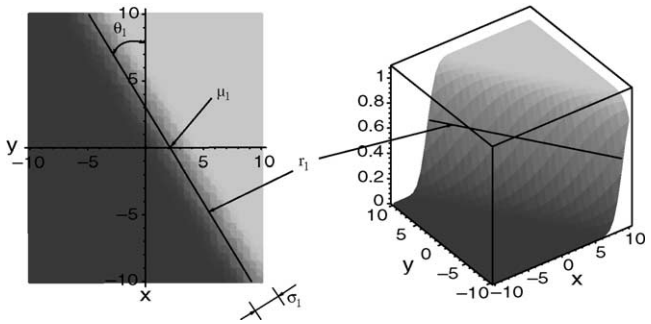

Fig. 1. These figures show the straight line and its main parameters superimposed to the unit step edge function model $U_x(I, P_x)$.

The graphical model of the USEF is the three-dimensional step edge shown in Fig. 1. This model describes completely the 2D intensity variations within a single equation instead of the two step process of convolving an ideal shaped gray value structure with a Gaussian filter as is normally done. In this way, it is straightforward to scale the model to the 2D intensity variations using the operations of addition and multiplication as follows:

$$U'_x(I, P_x) = U_x(I, P_x)A + B, \tag{3}$$

where A represents the distance between the lower and upper gray levels and B represents the lower gray value, also called here floor level. The unit step edge function $U_y(I, P_y)$ with respect to the y-axis is represented in a similar way, where all intervals of the variables remain the same and μ_2 designates the position y of the line that crosses the x-axis. The rotation θ_2 designates the orientation of the unit step edge model in the y direction. $U_y(I, P_y)$ can be evaluated numerically using the Gaussian error function as follows:

$$U_y(I, P_y) = \pm\frac{1}{2}\mathrm{erf}\left(\frac{(y - x\cdot\tan(\theta_2) + \mu_2)}{\sigma_2\sqrt{2}}\right) + \frac{1}{2}. \tag{4}$$

Hence, the USEF $U_y(I, P_y)$ is characterized by a r_2 straight line along its main direction. The straight line equation is obtained from the numerator in the argument of the exponential function, see Fig. 1.

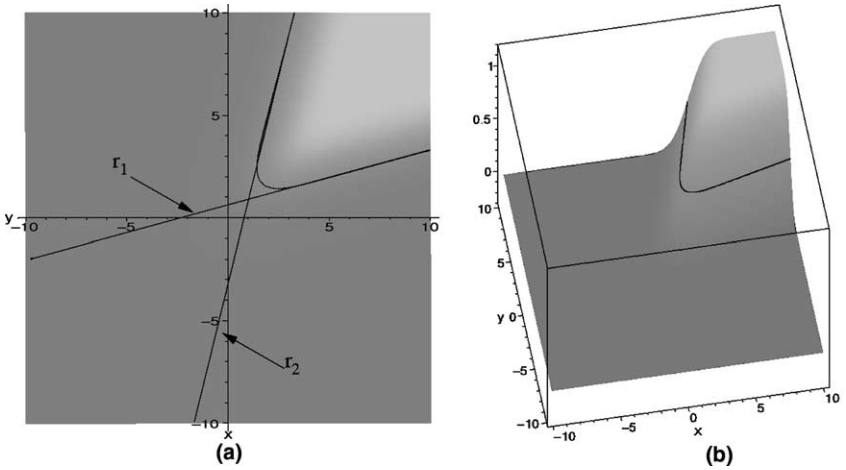

Fig. 2. Corner Unit Function $M_L(x, y, \vec{P})$ built from two USEF's. (a) Top view of the CUF model showing both straight lines, r_1 and r_2, along both edges. (b) Three-dimensional view of the corner, as well as the central contour curve.

3. L-corner modeling

L-corners are generated when two straight-line edges join into a single point creating two homogeneous gray zones with different intensities, see Fig. 2. This work proposes a new corner modeling based on the USEF model. In order to obtain a Corner Unit Function (CUF), two USEF's are multiplied as follows:

$$M'_L(x,y,\vec{P}) = U_x(I,P_x)\cdot U_y(I,P_y)\cdot A + B. \tag{5}$$

The structure generated by Eq. (5) is known in the literature as the "L-corner". The parameters σ_1, θ_1, μ_1, σ_2, θ_2, μ_2, $A\times B$, represent the physical and geometrical contours of an L-corner. Therefore, in order to obtain the corner model, we simply multiply both USEF's. In summary, our model

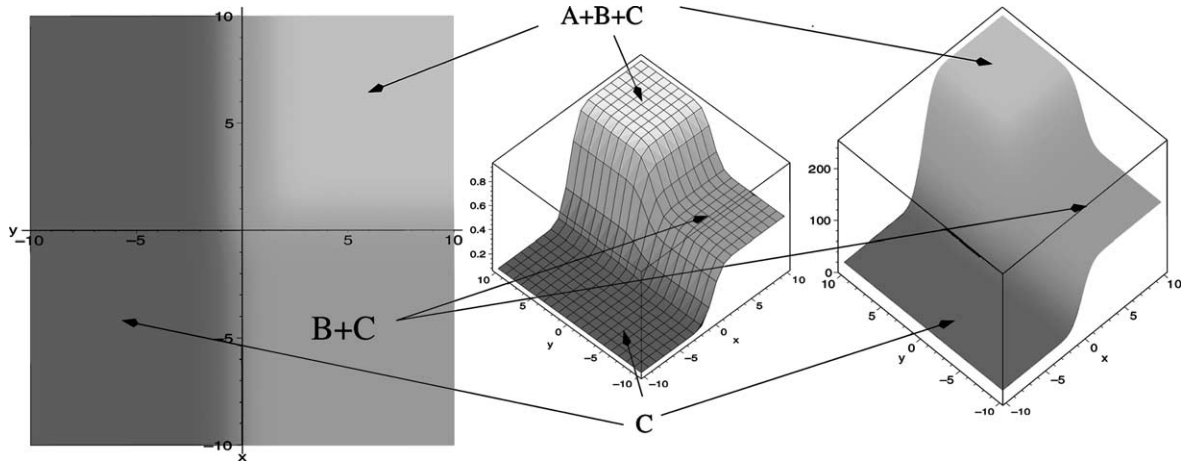

Fig. 3. The vertex model can be easily obtained from an L-corner model and a third USEF.

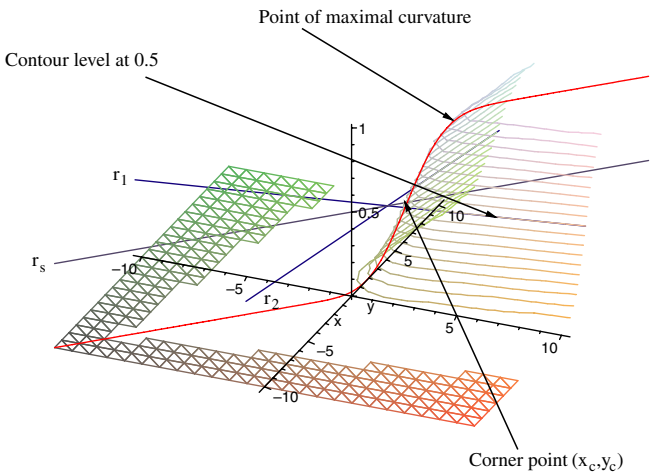

Fig. 4. This figure shows the exact position of the L-corner point we are searching for along the r_s straight line that is changing its orientation between the r_1 and r_2 straight lines.

is based on an analytical expression with the following characteristics:

1. Each edge on the corner has different levels of blurring. This is physically produced by the non-square CCD pixels of the Pulnix 9701 camera. Hence, the CUF models the degree of blurring along each edge.
2. Each edge is independent. Therefore, there is not any restriction with respect to the acute or obtuse of the angles within the corner.
3. The corner moves freely around the explored window. We obtain the position and orientation of the corner around any point within the studied window.
4. The gray levels are self-adjusted inside and outside of the corner.

4. Extraction of multiple features

Considering the above procedure for building L-corners, it is possible to model arbitrary complex gray value structures in terms of the unit step edge function by means of simple addition and multiplication operations. The total number of parameters used by the model is in general:

$$n = 3 + 2N + O, \tag{6}$$

where the first three, in the case of the L-corner, are given by the amount of blur σ and the lower and upper gray values A and B, respectively; N represents the number of step edge models, and O specifies the number of operations used to represent the feature. In fact, the first three should be increased if we take into account different blurs for each main direction and multiple gray values when considering more complex models. For example, the vertex model needs an extra gray level, and in total we need twelve parameters to model the corner, see Fig. 3. A vertex model (VUF) can be easily obtained from an L-corner model (CUF) and a third USEF as follows:

$$V'(I,P) = U_x(I,P_x)\cdot U_y(I,P_y)\cdot A + U_z(I,P_z)\cdot B + C. \tag{7}$$

5. Displacement of the L-corner

In this section, we describe the L-corner localization procedure, considering that we have already solved the process of fitting the general model to intensity variations (Olague et al., 2003). Calculation of partial derivatives through analytical expressions is made with the Maple package. The displacement of the L-corner is produced by the blurring effect introduced by the bandlimited CCD sensors and the angle between both lines. The USEF model considers a straight line that characterizes the position and orientation of each edge composing the corner, as well as the blurring. The straight lines are given by: $x - y\cdot\tan(\theta_1) - \mu_1$, along the x-axis, and $y - x\cdot\tan(\theta_2) - \mu_2$, along the y-axis. These two expressions are obtained from

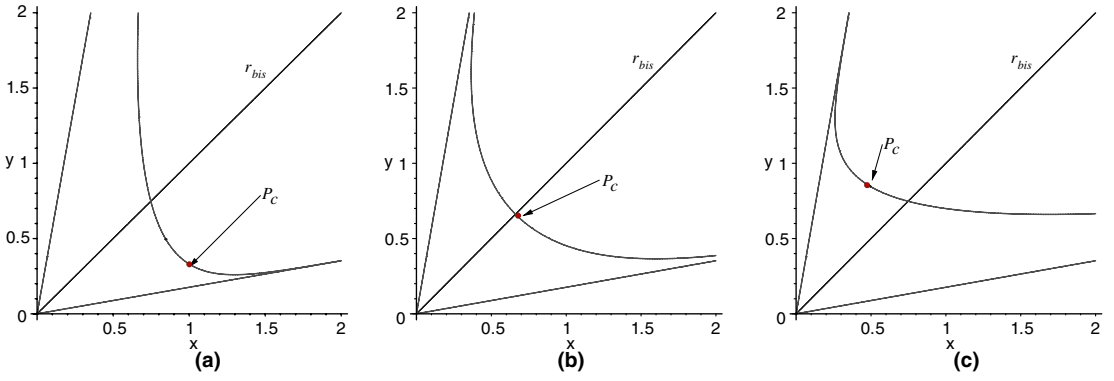

Fig. 5. Curve distortion using several blur factors: (a) $\sigma_1 = 0.5$, $\sigma_2 = 4.0$, (b) $\sigma_1 = \sigma_2 = 1.0$, (c) $\sigma_1 = 4.0$, $\sigma_2 = 0.5$.

the numerators in the arguments of the exponential functions. The point of intersection (x_0, y_0) at which the two lines meet is given by

$$\left(x_0 = \frac{\tan(\theta_1)\mu_2 + \mu_1}{-1 + \tan(\theta_2)\tan(\theta_1)}, \right.$$
$$\left. y_0 = \frac{\tan(\theta_2)\mu_1 + \mu_2}{-1 + \tan(\theta_2)\tan(\theta_1)} \right). \quad (8)$$

Each straight line is asymptotic to the contour level $C(I,P) = 0.5$, as shown in Fig. 4. Each straight line may be seen as defining a vector. Using both vectors and the scalar or inner product we can calculate the angle between both straight lines. Our goal is to find the corner point (x_c, y_c). Since our problem is defined geometrically, we can define a line that crosses the intersection point and lies between the two lines that characterize the

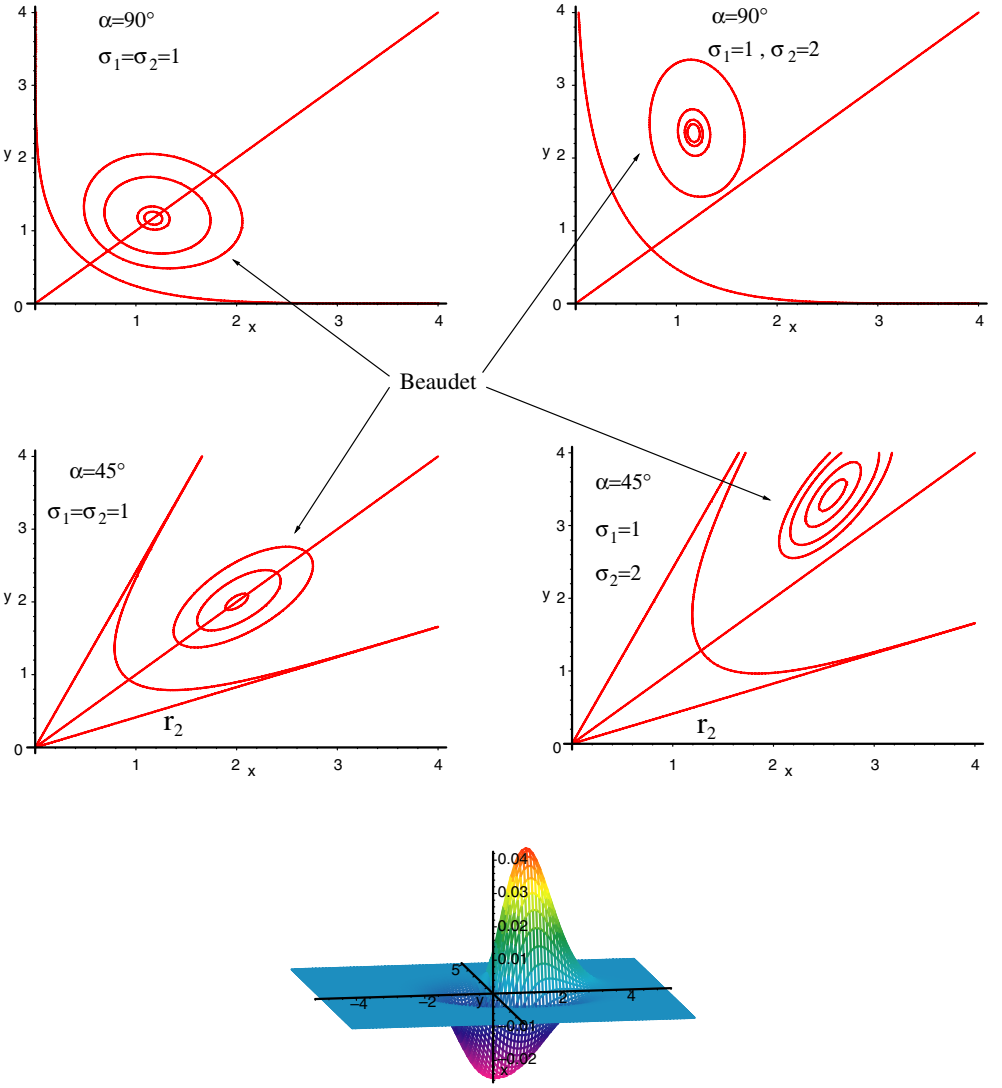

Three–dimensional view of the Beaudet criterion applied to our L–corner model

Fig. 6. Exact Beaudet (1978) corner position using several blur factors and aperture angles.

L-corner. The corner should be at the point where $C(I,P) = 0.5$. We can now (numerically) calculate the position that satisfies the above implicit equation using the algorithms of bracketing and bisection. However, we still need to find the best point along the implicit curve that defines the exact place for the L-corner. In order to solve this problem, we use the downhill simplex method for searching the point that minimizes the Euclidean distance $D_{\min}$ between the intersection point and the corner point. The exact corner point will then be the point that minimizes the distance $D_{\min}$ and satisfies the implicit equation $C(I,P) = 0.5$. Traditionally, the position of the L-corner point that is searched for by direct and indirect corner detector approaches is defined as the point of maximum curvature of linked edge points, and just one blur factor is considered in the analysis. Deriche (1993) reports that the corner is found at the point where the Laplacian is zero. Fig. 4 is a three-dimensional representation of our model that illustrates graphically our criterion for localizing the

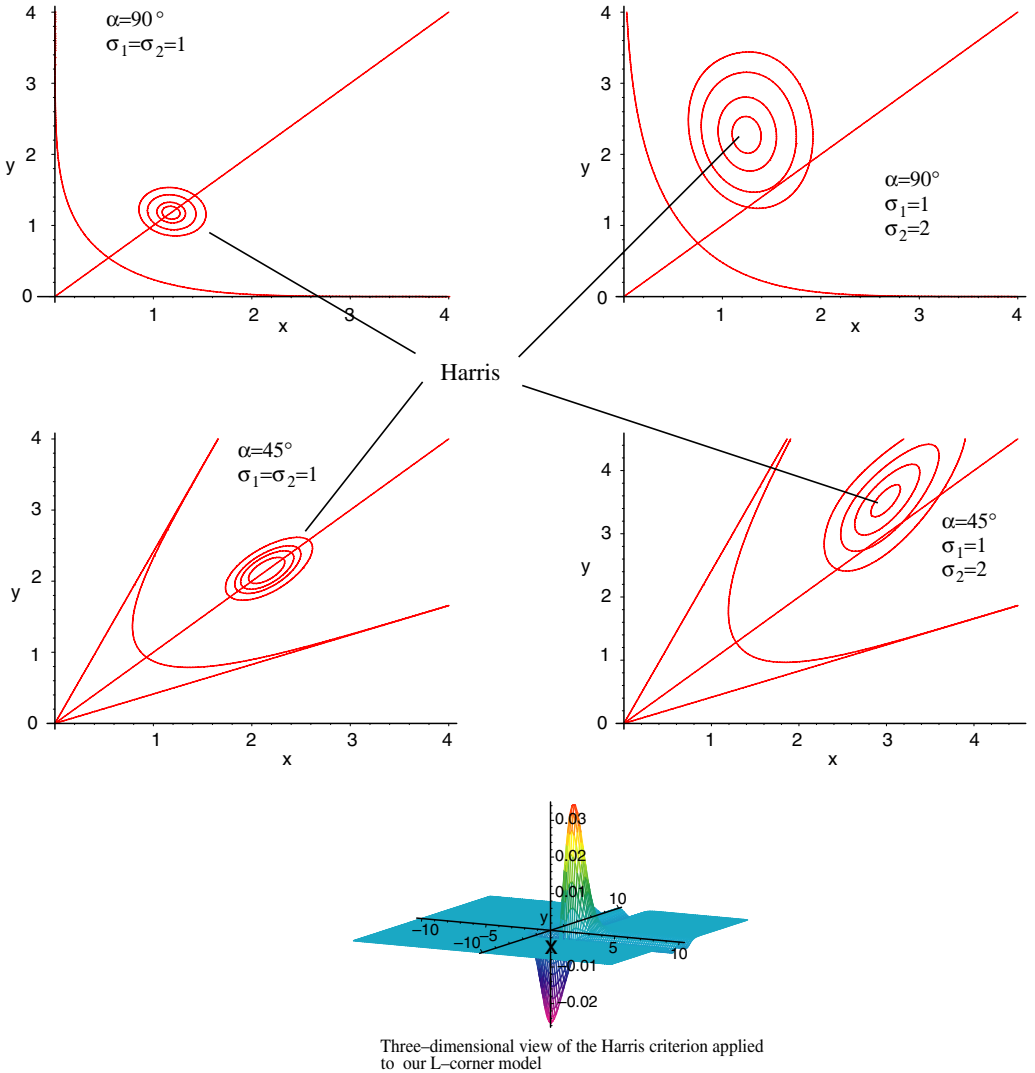

Fig. 7. Exact Harris (1988) corner position using several blur factors and aperture angles.

exact position of the L-corner point. It is evident that the point of maximum curvature has a symmetric point located at the lower part of the corner. Considering this fact, we propose by geometry that the middle point along the curve that goes from top to bottom satisfies in an optimal manner the exact position of the L-corner point. Our modeling takes into account that a corner can be displaced due to the different blurs produced by the shape and size of the photosensitive elements within a CCD image sensor. Because each USEF is independent of each other there is not any restriction about the corner morphology; for example, about how acute or obtuse the angle between both straight lines is. Moreover, the L-corner can be moved around the complete window being explored.

6. Comparing the CUF model with previous L-corner detectors

In this section, we compare the proposed CUF model with previous L-corner detectors. Fig. 5 shows the behavior of corner location considering several blur factor sets. Clearly, the corner is displaced with respect to the bisector line when both factors are different. Our goal here is to show the differences and similarities of the corner location used by Beaudet (1978), Dreschler and Nagel (1982), Kitchen and Rosenfeld (1982), Deriche and Giraudon (1993), and Rohr (1992), to the criterion proposed in this paper. With this, we expect to provide confidence on the usefulness of our approach.

The first three detectors proposed for comparison were developed for pixel resolution. Nevertheless, the criteria can be applied to our L-corner model for the purpose of contrasting the differences and similarities. Beaudet (1978) proposed a rotationally invariant operator based on the determinant of the Hessian associated to the image. Fig. 6 shows the behavior of the detector considering four blur factor sets. As a result, we observe that the L-corner location is displaced towards the top of the corner. Considering only one blur factor, the maximum (corner) of the Beaudet function is found along the bisector line r_{bis}. On the other hand, if we consider different blur factors, the corner is found between the r_{bis} and r_1 lines. However, our criterion find the corner between the r_{bis} and r_2 lines with a less important displacement. Based on these results, we can consider the detector proposed by Beaudet as different to the proposed in this paper. Beaudet's corner detector is unstable with respect to the aperture angle and blurring factors. Harris detector is another well-known operator, which could be considered as a variant of the Beaudet corner detector, see Fig. 7. The operator proposed by Harris and Stephens (1988) adds a fraction of a variant of the Laplacian to the Beaudet's criterion using what is known as the Harris constant; k which lies in the interval $[0, \frac{1}{4}]$. Fig. 7 shows the detector with the Harris constant $k = 0.04$, which is normally reported in the literature. We can observe the similarity with

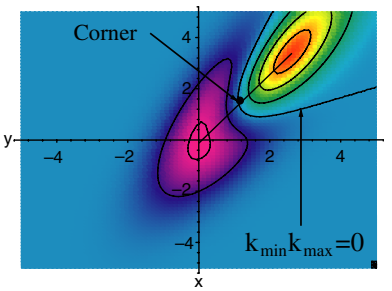

Aerial view of the D&N criterion applied to our L–corner model

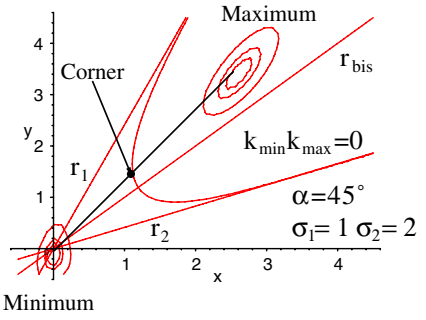

Fig. 8. Exact Dreschler and Nagel (1982) corner position using an aperture angle of 45° and blur factors of $\sigma_1 = 1.0$ and $\sigma_2 = 2.0$.

Beaudet's corner detector. If we employ a bigger value the location of the corner, for the case of different blurring factors, is moved towards the bisector line. However, in practice it is harder to define a threshold because the maximum tends to zero. This is the main reason to use a small value for the constant, and as a result we obtain a behavior similar to Beaudet's corner detector. Dreschler and Nagel (1982) proposed an operator based on the Gaussian curvature principle. In order to locate the corner, two points (maximum and minimum) are first located, then the point between both points where the principal curvature crosses zero is designated as the corner. Fig. 8 shows the behavior of the corner detector. Dreschler and Nagel's corner detector suffers from the same undesirable characteristics as Beaudet's detector. Kitchen and Rosenfeld (1982) proposed a measure of cornerness based on an operator that corresponds to the curvature scaled by the gradient magnitude. Fig. 9

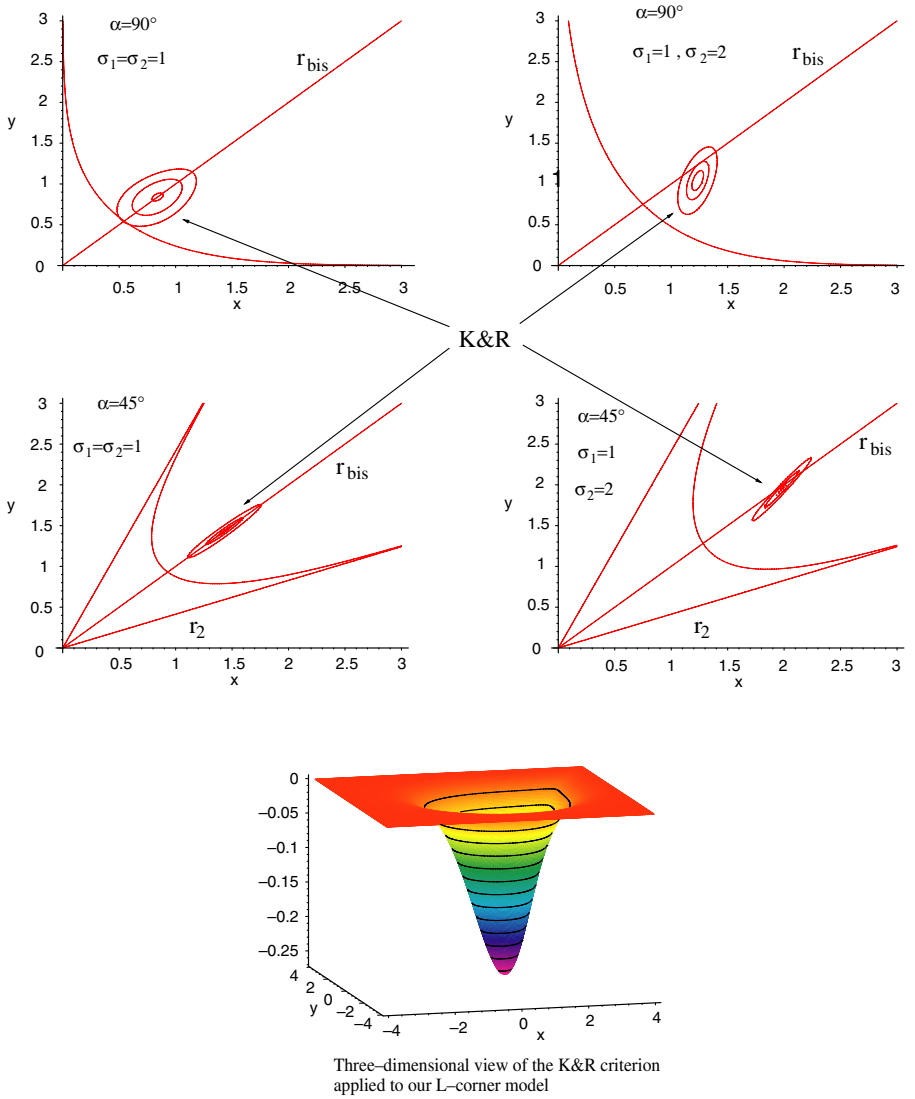

Fig. 9. Exact Kitchen and Rosenfeld (1982) corner position using several aperture angles and blur factors.

shows the behavior of the operator with respect to the implicit contour curve $C(I,P) = 0.5$, the aperture angle, as well as different blur factors. We observe that the corner location is displaced towards the top of the corner. Considering only one blur factor, we found the corner along the bisector line. Considering different blur factors, the corner is found between the r_{bis} and r_2 lines. In summary, Kitchen and Rosenfeld's detector agrees well with our criterion for corner location. However, it is still different from the point of view of displacement.

Deriche and Giraudon (1993) studied analytically the behavior of corners in the scale space. They proposed an approach in order to correct the displacement of corner position as follows: Firstly, a Laplacian image is calculated; Secondly, Beaudet's measure at two scales is calculated and an extrema detection in all directions is performed. Around each detected extrema in the image corresponding to the first scale we look in the second image for the position of the local maximum. Once this second maximum is detected, we look for the exact position of the corner as the point that belongs to the line segments joining the two positions and where a zero crossing occurs in the Laplacian image. Fig. 10 shows the behavior of the proposed algorithm. We observe that the line joining both extrema is the bisector line r_{bis}. The corner location is displaced along the bisector line at zero-crossing with respect to the aperture angle. In summary, the approach proposed by Deriche and Giraudon defines the location of the corner biased towards the corner floor and this behavior is in general contrary to the approach proposed in this paper. Finally, Rohr's detector is analyzed using an implicit equation, as we have made here in a similar way. The position of the corner point is independent of the height between the floor

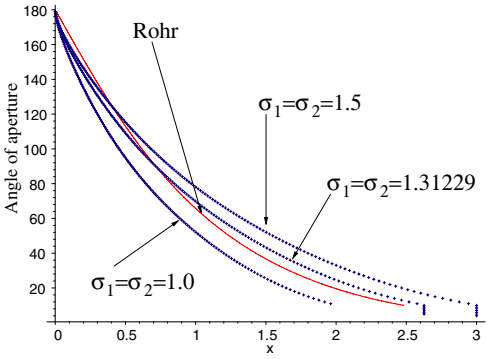

Fig. 11. Displacement of Rohr's corner position with respect to the aperture angle, together with that of our model, using several blur factors.

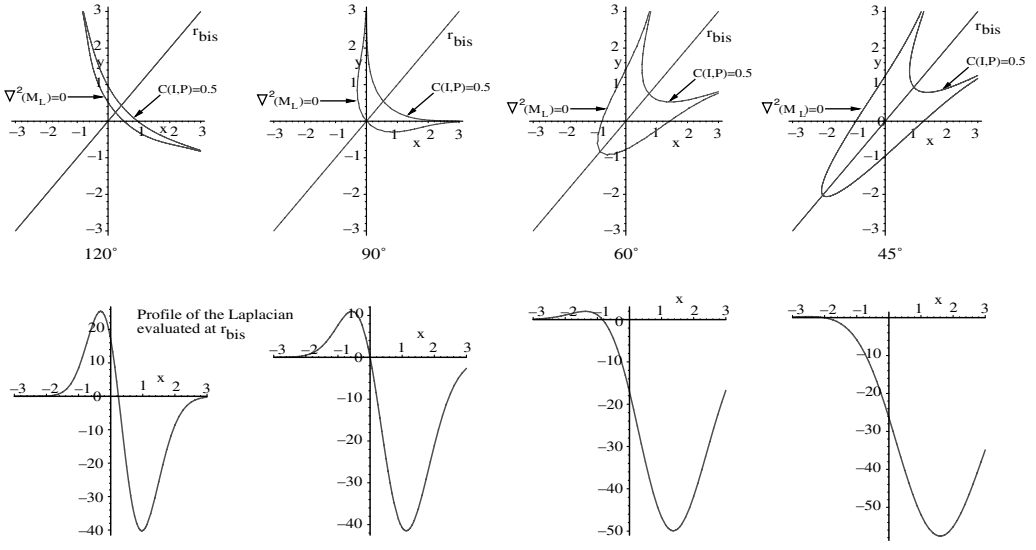

Fig. 10. Zero crossing behavior of the Laplacian using different aperture angles.

Table 1
Intrinsic parameters computed with the K&R corner detector

Image	α_u	α_v	u_0	v_0
1	−846.993	983.218	303.491	321.515
2	−832.861	968.630	351.668	343.830
3	−736.878	854.779	293.159	330.854
4	−811.104	936.987	295.140	348.316
5	−864.280	1000.831	319.202	351.686
6	−880.103	1022.265	304.188	320.721
7	−870.797	1011.478	312.025	314.904
8	−828.918	957.628	334.481	347.584
9	−864.280	1000.831	319.202	351.686
10	−896.779	1035.635	282.617	393.257
11	−925.399	1072.833	294.138	330.264
12	−807.135	931.533	290.416	373.279
13	−755.350	874.399	309.405	333.144
14	−852.554	985.909	295.963	379.274
15	−864.280	1000.831	319.202	351.686
16	−778.400	899.715	314.562	345.037
17	−852.084	988.060	295.830	351.447
18	−875.877	1015.967	318.835	350.058
19	−846.993	983.218	303.491	321.515
20	−891.603	1035.749	295.469	348.970
Average	−844.133	978.024	307.624	345.451
Std. dev.	47.314	55.414	16.538	20.119

Table 2
Extrinsic parameters computed with the K&R corner detector

Image	R_x (°)	R_y (°)	R_z (°)	t_x	t_y	t_z
1	−44.211	88.770	87.517	−76.932	−19.325	1335.515
2	−45.996	−87.063	−89.564	−1.443	−50.015	1322.154
3	−45.067	88.155	87.152	−93.080	−32.356	1172.176
4	−45.942	87.676	86.888	−90.189	−55.747	1274.937
5	−46.040	89.881	88.478	−52.698	−60.153	1357.286
6	−44.132	88.762	87.703	−76.034	−18.436	1380.355
7	−44.168	89.505	88.221	−63.747	−11.172	1368.154
8	−45.908	−88.436	89.676	−28.486	−55.019	1309.098
9	−46.040	89.881	88.473	−52.698	−60.153	1357.286
10	−47.890	86.161	85.611	−109.779	−115.167	1400.506
11	−44.083	87.789	87.024	−91.790	−30.072	1445.175
12	−47.756	87.310	86.548	−97.410	−90.335	1270.564
13	−45.246	89.652	88.235	−67.161	−35.832	1198.571
14	−47.890	87.799	86.910	−88.806	−97.646	1338.165
15	−46.039	89.881	88.473	−52.698	−60.153	1357.286
16	−46.070	89.237	87.882	−59.996	−51.912	1233.276
17	−46.030	88.184	87.242	−88.858	−59.749	1340.254
18	−46.072	89.796	88.412	−53.321	−57.923	1374.145
19	−44.211	88.770	87.517	−76.933	−19.325	1335.515
20	−46.105	88.078	87.166	−89.490	−56.626	1398.305
Average	−45.745	70.989	78.778	−70.577	−51.856	1328.436
Std. dev.	1.199	54.297	39.633	25.865	27.089	68.771

Table 3
Intrinsic parameters computed with our subpixel L-corner detector

Image	α_u	α_v	u_0	v_0
1	−1227.650	1423.887	271.864	312.546
2	−1203.922	1395.749	251.808	315.922
3	−1224.606	1420.150	264.743	312.448
4	−1186.412	1375.804	260.305	331.596
5	−1201.286	1392.345	259.250	329.104
6	−1203.045	1395.538	257.157	329.216
7	−1212.283	1404.637	257.471	321.710
8	−1194.971	1385.369	251.021	309.744
9	−1214.887	1408.786	264.843	316.562
10	−1211.432	1402.922	260.937	335.604
11	−1220.388	1415.321	258.674	331.163
12	−1238.196	1435.989	264.449	316.855
13	−1193.260	1383.388	259.044	307.829
14	−1220.710	1415.299	261.779	320.159
15	−1200.134	1390.995	262.161	316.468
16	−1188.114	1377.768	263.115	314.110
17	−1202.620	1393.061	260.728	335.080
18	−1198.986	1391.049	255.844	324.630
19	−1225.430	1422.130	254.520	324.977
20	−1205.959	1398.660	262.133	326.343
Average	−1208.715	1401.442	260.092	321.603
Std. dev.	14.088	16.501	4.827	8.545

Table 4
Extrinsic parameters computed with our subpixel L-corner detector

Image	R_x (°)	R_y (°)	R_z (°)	t_x	t_y	t_z
1	−43.347	85.701	85.459	−127.632	−5.408	1869.182
2	−43.376	84.432	84.574	−157.956	−9.754	1832.566
3	−43.420	85.099	85.017	−138.472	−5.422	1863.712
4	−44.188	84.986	84.937	−144.994	−30.52	1809.016
5	−44.053	84.833	84.812	−146.641	−27.198	1828.878
6	−44.067	84.757	84.780	−149.760	−27.406	1832.592
7	−43.779	84.754	84.741	−149.266	−17.581	1844.007
8	−43.000	84.410	84.574	−159.207	−1.549	1819.528
9	−43.523	85.337	85.165	−138.044	−10.732	1850.081
10	−44.277	84.871	84.892	−144.155	−35.704	1843.106
11	−44.080	84.763	84.775	−147.563	−29.877	1857.204
12	−43.536	85.326	85.181	−138.660	−11.043	1883.319
13	−43.131	84.910	84.898	−147.006	0.722	1818.024
14	−43.636	85.179	85.086	−142.738	−15.391	1857.989
15	−43.560	84.991	84.965	−142.364	−10.583	1827.936
16	−43.462	85.152	85.065	−140.785	−7.618	1810.859
17	−44.324	84.953	84.916	−144.370	−35.063	1830.541
18	−43.899	84.608	84.686	−151.849	−21.336	1827.106
19	−43.782	84.599	84.661	−153.789	−21.656	1865.275
20	−43.910	85.097	84.974	−142.227	−23.562	1837.346
Average	−43.718	84.938	84.908	−145.374	−17.334	1840.413
Std. dev.	0.378	0.318	0.220	7.315	11.237	20.553

and the top of the corner. There is a linear relationship between the blur factor and the exact position of the corner point. All the considerations reported by Rohr agree with and are observed in the behavior of our criterion for corner detection. Fig. 11 shows the displacement of position x with respect to the aperture angle. The purpose of this figure is to compare Rohr's criterion and our criterion, using several blur factors. In general, using angles larger than 90°, our criterion provides a smaller displacement, while for angles smaller than 90°, the opposite occurs.

Finally, we compare our L-corner algorithm with the K&R corner detector using a well-know camera calibration algorithm proposed by Faugeras and Toscani (1986, 1987). The camera is a Pulnix TM-9701d with a C-mount lens Fujinon, HF16A-2M1, of focal length $f = 16$ mm. The pixel size of the camera is $11.6\,\mu m \times 13.6\,\mu m$. Tables 1 and 2 show the average and standard deviation that we have obtained with the K&R corner detector, after calibrating the camera with a sequence of 20 images (see Fig. 12). If we contrast now the results with those obtained in Tables 3 and 4, it is evident the advantage of using an accurate subpixel detector. The accuracy is greatly improved as we can see on all intrinsic and extrinsic parameters. It is remarkable also the difference that is obtained on the intrinsic and extrinsic average values. This experiment shows the importance of using a reliable L-corner detector, since it is really the accurate determination of object coordinates which should be the primary aim in camera calibration, as well as on many other computer vision tasks.

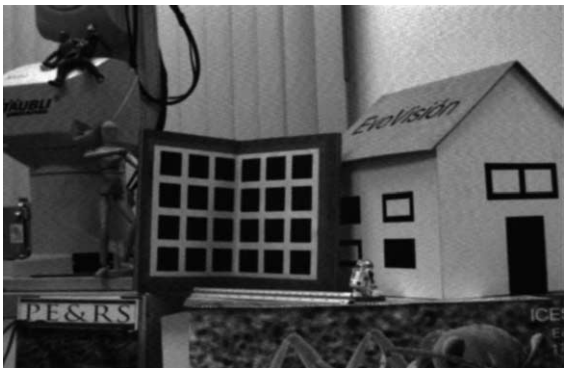

Fig. 12. Twenty images were captured with a Pulnix TM-9701 digital camera using a Fujinon lens of focal length $f = 16$ mm, in order to calibrate the camera using our L-corner detector.

7. Conclusion

This paper has introduced a new basic function, that due to its simplicity, is able to build complex corners. This function was called Unit Step Edge Function, USEF, and it defines a straight line edge. The USEF is a distribution function that models the optical and physical characteristics of digital imaging systems. A new criterion for precise L-corner location was introduced. In comparison to our model, Beaudet's, Dreschler and Nagel's, and Kitchen and Rosenfeld's detectors located the exact position of the corner upwards towards the top of the corner, while Deriche and Giraudon's located the exact position of the corner point biased downwards towards the floor of the corner. The displacement is contrary to our criterion, $C(I, P) = 0.5$, considering the aperture angle. On the other hand, the criterion proposed by Rohr (1992) produces a similar behavior to that of our model, considering the curve of displacement plotted by the corner position along the x-axis; see Fig. 11. Both criteria are similar, but arise from very different concepts: our criterion is based on purely geometric reasoning, while the criterion proposed by Rohr employs concepts from differential geometry. These last two detectors were studied here considering equal blur factors along the two main directions for the purpose of comparison. However, our model can use different blurs, as can arise in the case of a rectangular CCD. Modeling complex corners and extracting a rich set of information is our main goal for future research.

Acknowledgments

This research was funded by CONACyT Mexico and INRIA France through the LAFMI pro-

ject. First author gratefully acknowledges the support of Ministerio de Ciencia y Tecnología, Spain, research project number TIC2002-04498-C05-01 granted when Dr. Olague was a visiting professor at the Universidad de Extremadura in Merida.

References

Ackermann, F., 1984. Digital image correlation: performance and potential application in photogrammetry. Photogramm. Rec. 11 (64), 429–439.

Baker, S., Nayar, S.K., Murase, H., 1998. Parametric feature detection. Int. J. Comput. Vis. 27(1), 27–50, Kluwer Academic Press.

Beaudet, P.R., 1978. Rotationally invariant image operators. In: Proc. Int. Conf. Pattern Recognition, pp. 579–583.

Canny, J., 1986. A computational approach to edge detection. IEEE Trans. Pattern Anal. Machine Intell. 8 (6), 679–698.

Deriche, R., 1987. Using Canny's criteria to derive a recursively implemented optimal edge detector. Int. J. Comput. Vis. 1 (2), 167–187.

Deriche, R., Giraudon, G., 1993. A computational approach for corner and vertex detection. Int. J. Comput. Vis. 10(2), Kluwer Academic Press, pp. 101–124.

Dreschler, L., Nagel, H., 1982. On the selection of critical points and local curvature extrema of region boundaries for interframe matching. In: Proc. Int. Conf. Pattern Recognition, pp. 542–544.

Faugeras, O.D., Toscani, G., 1986. The calibration problem for stereo. Proc. Comput. Vis. Pattern Recognit. 15–20. Miami Beach, Florida, USA, June.

Faugeras, O.D., Toscani, G., 1987. Camera calibration for 3D computer vision. In: Proc. Int. Workshop on Machine Vision and Machine Intelligence, Tokyo, Japan, February.

Foerstner, W., 1986. A feature based correspondence algorithm for image matching. Int. Arch. Photogramm. Remote Sens. 26 (3), 150–166.

Gruen, A.W., 1985. Adaptive least squares correlation: a powerful image matching technique. South Afr. J. Photogramm., Remote Sens. Cartogr. 14 (3), 175–187.

Gruen, A., Baltsavias, E.P., 1988. Geometrically constrained multiphoto matching. Photogramm. Eng. Remote Sens. 54 (5), 633–641.

Harris, C., Stephens, M., 1988. A combined corner and edge detector, Fourth Alvey Vision Conference, pp. 147–151.

Kitchen, L., Rosenfeld, A., 1982. Gray-level corner detection. Pattern Recognition Lett. 1 (2), 95–102.

Marr, D., Hildreth, X., 1980. Theory of edge detection. Proc. Roy. Soc. Lond. B 207, 187–217.

Medioni, G., Yasumoto, Y., 1987. Corner detection and curve representation using cubic B-splines. Comput. Vis., Graphics Image Process. 39, 267–278.

Mehrotra, R., Nichani, S., 1990. Corner detection. Pattern Recognition 23 (11), 1223–1233.

Moravec, H.P., 1977. Towards automatic visual obstacle avoidance. In: Proc. 5th Int. Joint Conf. on Artifcial Intelligence, Cambridge, Massachusetts, USA, p. 584.

Lindeberg, T., 1998. Feature detection with automatic scale selection. Int. J. Comput. Vis., Vol. 30, No. 2, pp. 79–116. Kluwer Academic Publishers.

Olague, G., Hernández, B., 2002. Flexible model-based multicorner detector for accurate measurements and recognition. In: 16th Int. Conf. on Pattern Recognition. IEEE Computer Society Press, Vol. 2, pp. 578–583, 11–15 August. Québec, Canada.

Olague, G., Hernández, B., Dunn, E., 2003. Hybrid evolutionary ridge regression approach for high-accurate corner extraction. In: IEEE Computer Society Conf. on Computer Vision and Pattern Recognition, Vol. 1, pp. 744–749, 18–20 June, Madison, Wisconsin, USA.

Olague, G., 2002. Automated photogrammetric network design using genetic algorithms. Photogrammetric Engineering & Remote Sensing. Vol. 68. No. 5, pp. 423–431. May. Paper Awarded the "2003 First Honorable Mention for the Talbert Abrams Award" by ASPRS.

Rohr, K., 1992. Modelling and identification of characteristic intensity variations. Image Vis. Comput. 10 (2).

Rohr, K., 1992. Recognizing corners by fitting parametric models. Int. J. Comput. Vis., Vol. 9, No. 3, pp. 213–230. Kluwer Academic Press.

Rosin, P.L., 1996. Augmenting corner descriptors. Graphical Models Image Process. 58 (3), 286–294.

Tsai, D.M., Hou, H.T., Su, H.J., 1999. Boundary-base corner detection using eigenvalues of covariance matrices. Pattern Recognition Lett., Vol. 20, pp. 31–40. Elsevier.

Zheng Z., Wang, H., Teoh, E.K., 1999. Analysis of gray level corner detection. Pattern Recognition Lett. Elsevier, pp. 149–162.